ARTICLE

Half-Solidity of Tetrahedral-like Al_{55} Clusters

Joongoo Kang[†] and Yong-Hyun Kim[†,‡,*]

[†]National Renewable Energy Laboratory, Golden, Colorado 80401 and [‡]Graduate School of Nanoscience and Technology (WCU), Korea Advanced Institute of Science and Technology, Daejeon 305-701, Korea

ABSTRACT A new dynamic melting state, which has both solid and liquid characteristics, is revealed from first-principles molecular dynamics simulations of Al_{55} clusters. In thermal fluctuations near the melting point, the low-energy tetrahedral-like Al_{55} survives through rapid, collective surface transformations—such as parity conversions and correlated diffusion of two distant vacancies—without losing its structural orders. The emergence of the collective motions is solely due to efficient thermal excitation of soft phonon modes at nanoscale. A series of spontaneous surface reconfigurations result in a mixture or effective flow of surface atoms as is random color shuffling of a Rubik's cube. This novel flexible solid state (termed as half-solidity) provides useful insights into understanding stability, flexibility, and functionality of nanosystems near or below melting temperatures.

KEYWORDS: aluminum clusters · stability · melting transition · DFT · molecular dynamics

Many finite cluster systems containing only a hundred or even fewer constituent elements (*e.g.*, electrons,[1] atoms,[2−12] molecules,[8,13] and amino acids[14−16]) can exhibit solidlike or liquidlike behavior. Melting of such small clusters (known as "magic melters") is characterized by a broad but noticeable peak in heat capacity, which separates the solidlike and liquidlike states. At sufficiently low or high temperatures away from the melting peak, a cluster manifests characteristics of its macroscopic counterpart; in a solidlike state, microscopically the constituent elements have fixed average positions in space relative to each other—they can vibrate thermally but cannot flow away from the average positions. In a liquidlike state, a cluster has no atomic ordering or shape, and its individual constituent particles ceaselessly move and diffuse. Regarding the broadened melting transition, however, the distinction between solidlike and liquidlike states becomes blurred, and the melting transition becomes a stochastic and dynamic phenomenon.[2−16]

The stochastic, dynamic nature of the broadened melting transition is closely related to functioning of many finite-size cluster systems in nature. For example, protein systems[15,16] act as enzymes just below their melting temperatures (~0.9 T_m), where a delicate balance exists between solidlike and liquidlike states. Reactivities of nanocatalysts are largely affected by the surface restructuring dynamics.[17] If temperature is too high, these systems are melted (or denatured) and lose all of their functionalities. In the opposite limit, they are frozen with all of their structural and chemical flexibility diminished. Thus, functional clusters should simultaneously have structural stability and flexibility, and this can take place during the early stages of the melting transition. The melting and near-T_m dynamics of cluster systems have been studied extensively over the last two decades,[2−16] with the identification of two characteristic melting behaviors: (i) dynamic coexistence[3,5,8] and (ii) "floater"-induced surface melting.[4,5,8] In the dynamic coexistence near T_m, atomic clusters can weave back and forth between multiple phases, including solidlike and liquidlike states. In the surface-melted state, a few surface atoms ("floaters") are detached or excited out of the surface and cause melting only of the surface layer through dynamic atomic exchanges with the remaining surface atoms. These nanofeatured meltings illuminate on the rich physics and chemistry during the broadened melting transition. However, it is not clear how structurally ordered solid systems can also have a structural flexibility at finite temperature and how the flexibility can be represented in terms of atomic motions.

Here, we reveal for the first time a flexible solid state of an atomic cluster with collective atomic excitations during the early

*Address correspondence to yong.hyun.kim@kaist.ac.kr.

Received for review November 1, 2009 and accepted December 30, 2009.

Published online January 7, 2010. 10.1021/nn901536a

stages of its melting. At temperature below T_m, a solidlike Al_{55} cluster undergoes spontaneous, collective structural transformations to another solidlike state but with different surface configurations. A series of such surface nanotransformations, governed by Brownian dynamics, induce a random mixture of surface atoms (Supporting Information, Movie 1). This process is analogous to the random color shuffling of a Rubik's cube at nanoscale through its *collective* face rotations (see Figure. S1 in the Supporting Information). Because the cube keeps its ordered shape between rotations, it is in a solidlike state. However, because the constituent colors keep flowing randomly, the cube is also in a liquidlike state. As temperature increases, the color shuffling of the ordered cube occurs more frequently as is in liquid. So, the cube or the Al_{55} cluster is in an atomistic lattice-liquid state with an exhibition of flexible solid characters.

RESULTS AND DISCUSSION

To unveil the mechanistic of half-solidity, we performed extensive first-principles molecular dynamics (MD) simulations of Al_{55} in a neutral state at various temperatures ranging from 130−1200 K, as shown in Figure 1a. From the obtained potential energy ensembles, we calculated a heat capacity with a quantum correction (Figure 1b and legend). The result reproduces most of the nanoscale melting features[7] such as shape, location (T_m = 625 K), and broadness of the melting peak. In contrast, the classical force-field calculations[9,10] failed to reproduce these features, indicating that, even if costly, only state-of-the-art first-principles calculations should be employed to describe atomistic thermal motions as well as ground-state structures of the aluminum clusters. Potential energy ensembles close to the transition region, for example at T = 550 K [0.9 T_m], show asymmetric features associated with the fore-mentioned cluster melting behaviors, compared to the normal distributions of solidlike or liquidlike regions.

Figure 2 shows the single long-run MD simulation at 550 K over 1.5 ns (500 000 MD steps) and its potential energy trajectory of an Al_{55} cluster. The MD started from an initially disordered high-energy cluster. After the initial 160 ps, the cluster is solidified to a stable, low-energy cluster state. The Al_{55} cluster in this stable state contains a tetrahedral pyramid core (Al_{10}) with face-centered cubic (fcc) atomic stacking. Even though the loosely stacked Al atoms on the surface undergo some structural change, the core Al_{10} is almost intact structurally by t = 940 ps. The common-core tetrahedral cluster cannot survive indefinitely because of a large thermal-fluctuation effect at 550 K, and thus melting starts to occur. A snapshot of the cluster at t = 960 ps clearly represents a disordered structure in a liquidlike state. The melted cluster is quickly resolidified to the common-core tetrahedral cluster state at around t =

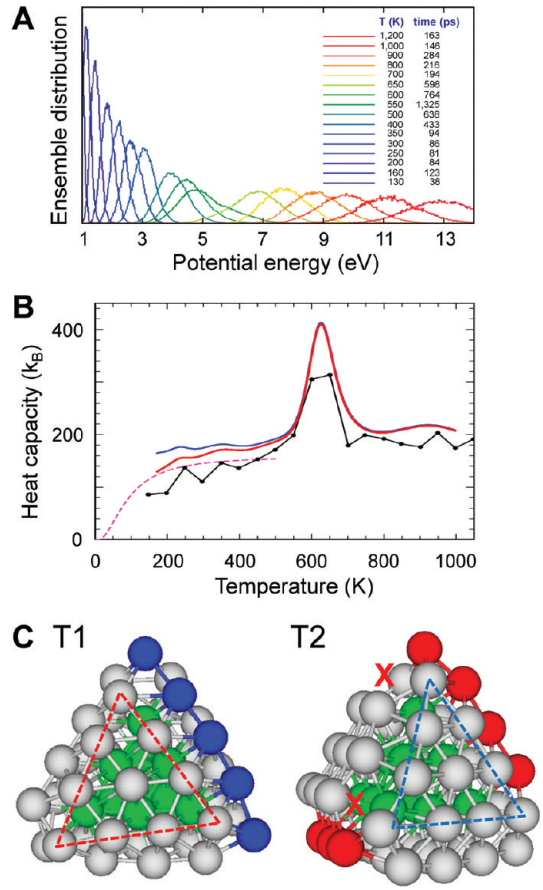

Figure 1. Heat capacity of tetrahedral-like Al_{55} clusters. (a) Normalized histograms of MD potential energy ensembles are shown for 16 simulation temperatures ranging from 130 to 1200 K. The potential energy is given with respect to the energy of the lowest-energy structure Al_{55}. In panel b, simulated classical heat capacity (blue line) from MD simulations is compared with experimental data (black dot and solid line) taken from ref 7. The classical heat capacity was calculated using the multiple-histogram method.[2,11] A quantum correction is added to the classical result (red line) based on the quantum heat capacity (pink dashed line) from the first-principles phonon spectrum (see the Supporting Information). (c) Two lowest-energy tetrahedral Al_{55} structures (T1 and T2) are shown. Both structures have a common core structure (Al_{10}, green) forming a tetrahedral pyramid with atomic stacking of a face-centered cubic (fcc) lattice. The core Al_{10} is covered with four fcc (111) facets (Al_{10}, gray) and one or two intervened rows between the (111) facets. In addition, the T2 structure contains two Al vacancies on the surface, positioned in the same facet as the most stable T2. The locations of vacancies are marked with X.

1040 ps. The finite lifetime (~800 ps) and back-and-forth switching of low- and high-energy states is known as the so-called *dynamic coexistence*.[3,5,8] We confirmed that the same tetrahedral Al_{10}-core clusters generally emerge, regardless of simulation temperature and initial structure.

Among the tetrahedral Al_{10}-core isomers observed, two lowest-energy Al_{55} (named as T1 and T2 hereafter) were identified, as shown in Figure 1c (see Figures S2 and S3 in the Supporting Information). Both the T1 and T2 clusters consist of the tetrahedral pyramid core, four fcc (111) surface facets, and intervened rows. At

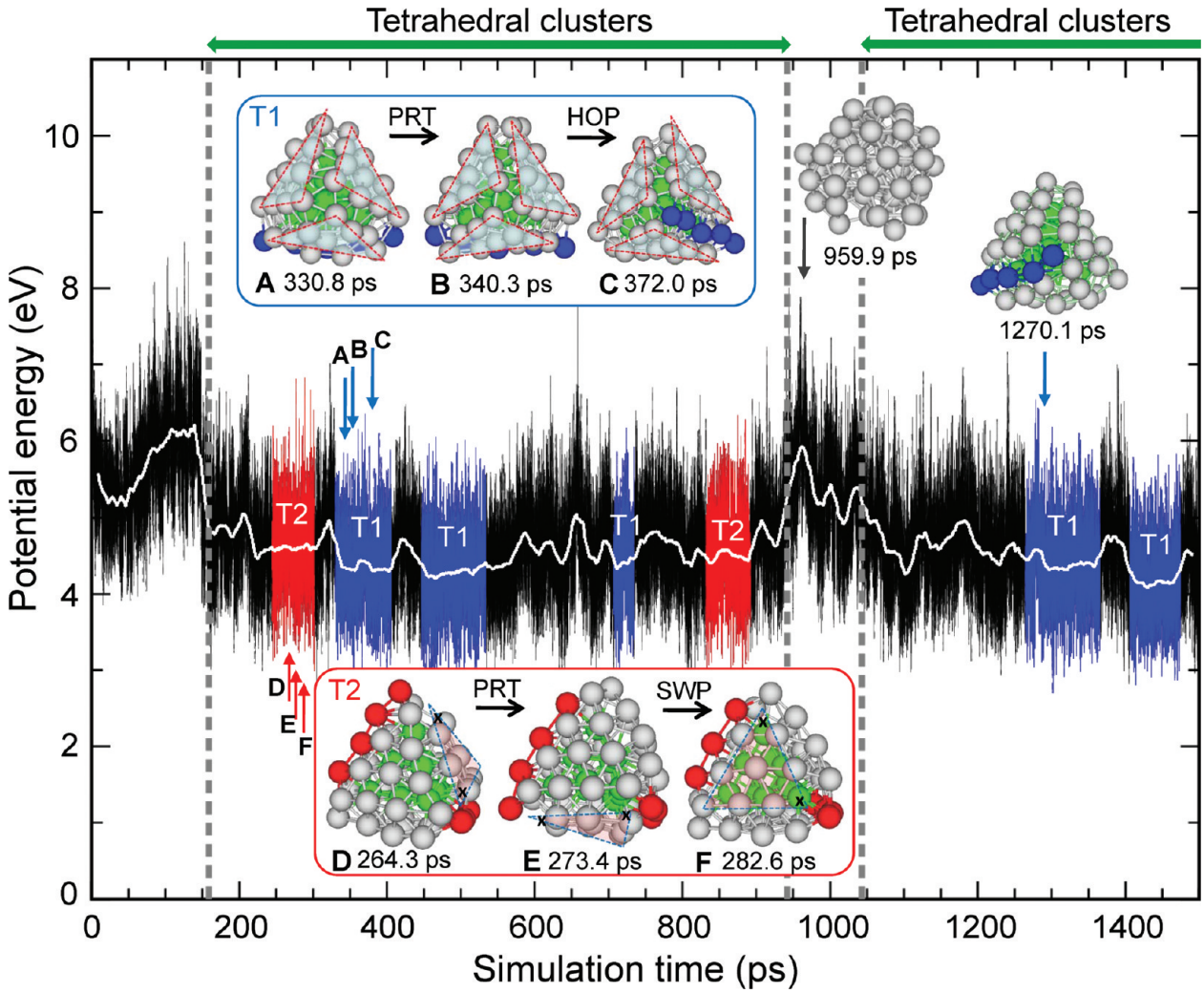

Figure 2. Nanocluster melting. Potential energies (black solid line) in an MD simulation at $T = 550$ K are shown with respect to the energy of the lowest-energy structure (T1). Short-time averages (white solid line) of the potential energy over a simulation period of 18 ps are also presented. Vertical dashed lines denote boundaries between a melted state (*e.g.*, snapshot at $t = 960$ ps) and a tetrahedral cluster state (*e.g.*, snapshot at $t = 1270$ ps). Blue- and red-colored regions within the tetrahedral cluster states represent time intervals in which T1 and T2 structures are observed. A series of snapshots demonstrates fast surface transformations of T1 and T2; helicity change (PRT) and intervened-row hopping (HOP) of T1 (a−c, upper inset); and parity change (PRT) and intervened-row swapping (SWP) of T2 (d−f, bottom inset).

zero temperature, the optimized T1 and T2 are nearly degenerate with an energy difference of E_{T2}-E_{T1} = 52 meV. The metastable T2 structure was independently proposed as the lowest-energy Al_{55} cluster based on the existing databases and their variations.[12] The simulated photoelectron spectrum of the tetrahedral-like clusters is in good agreement with experimental data[18] (see Figure S4 in the Supporting Information). T1 has one 5-atom intervened (dislocation) row at an edge of the core tetrahedron, and T2 has one 4-atom row at an edge and one 3-atom row at the opposite edge. In T1, each (111) surface facet is slightly tilted either clockwise or counterclockwise with respect to the underlying Al_{10} core facets to reduce stacking-fault stress on the surface. Thus, a helicity of T1 is defined. The T2, instead of having a helicity, possesses two Al vacancies on the surface to relax strain. Generally, the vacancy is stable at a corner of the triangular (111) facet, and the most stable T2 has the two vacancies in the same facet, as shown in Figure 1c. The vacancy near the 3-atom intervened row is relatively mobile so that it can easily migrate to other facets. The lowest-energy T1, T2 and their excited states with the tetrahedral core are henceforth referred to as "tetrahedral" clusters.

In Figure 2, the time intervals of the common-core tetrahedral cluster states are colored blue and red, which correspond to the T1 and T2 clusters, respectively. Noncolored time intervals represent common-core clusters, but with high-energy surface disordering. Such *surface melting* is initiated by thermal activation of weakly bonded Al atoms ("floaters") of tetrahedral cluster corners to the otherwise empty outer shell, as is in the typical surface melting process.[4,5,8] Thus, T1 or T2 has a finite lifetime of about 80 ps as colored. Once the surface is energetically excited, the cluster can relax to either T1 or T2, with more weight given to T1.

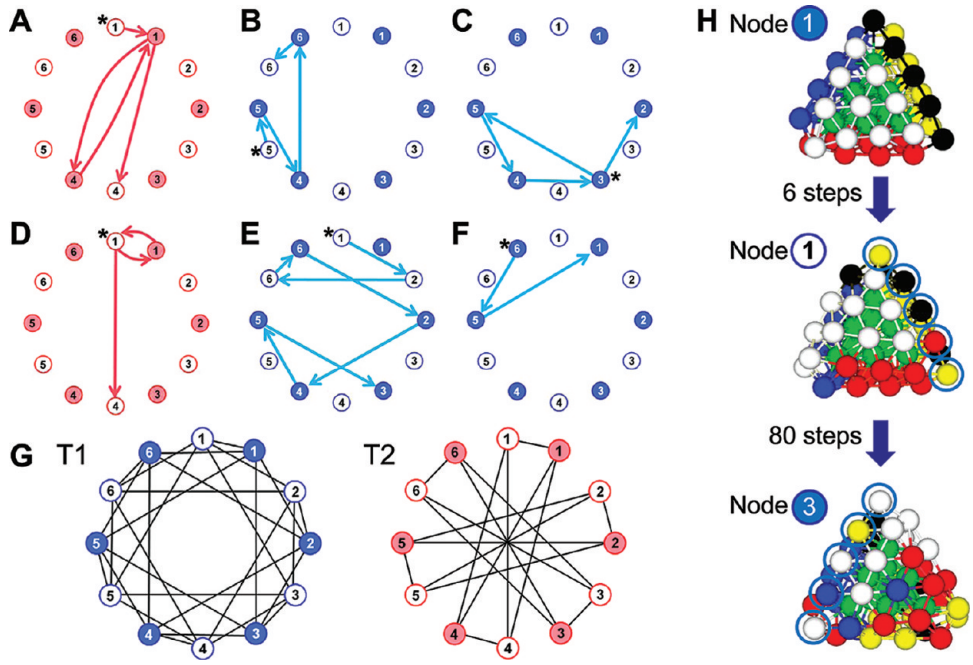

Figure 3. Confined Brownian motions in networks. The successive nanotransformations in the MD simulation at $T = 550$ K—colored blue and red in Figure 2—are represented as trajectories in a 12-node configuration space. Each node represents a different intervened-row position and parity of the tetrahedral Al_{55} clusters, T1 (b, c, e, f) and T2 (a, d). In each case, the starting node is marked with an asterisk (*). The six edges of the tetrahedral pyramid core are numbered by 1−6 to denote the position of the 5-atom (4-atom) intervened row in the T1 (T2) network. Two opposite nodes (*e.g.*, 1 and 4) correspond to two, non-neighbored, perpendicular edges of the tetrahedron. The open or filled node denotes the parity. For T2, we neglect migration of a mobile Al vacancy. (g) From the observed trajectories (a−f) and a 6-fold rotational symmetry between the open (or filled) nodes, two networks (T1 and T2) were constructed by connecting two nodes for a possible transition. Then, the collective transformational motion is represented as a random walk within the finite networks. (h) Three snapshots from a Monte Carlo simulation in the T1 network are depicted: steps 0 (top, node 1 and clockwise helicity), 6 (middle, node 1 and counterclockwise helicity), and 86 (bottom, node 3 and clockwise helicity). To visualize atomic movements during the successive nanotransformations, we colored the initial structure according to its nanodomains.

The Figure 2 insets show a series of snapshots of the tetrahedral clusters in the fixed frame of the core Al_{10}, demonstrating fast *nanotransformations* within T1 and T2. By analyzing the snapshots of T1 and T2, we identified four, two per each, independent transformational motions in terms of a change of helicity or a collective movement of vacancies and intervened rows. From $t = 331-340$ ps, the helicity of T1 changes from a counterclockwise to clockwise direction, as shown in Figure 2a,b; we named the motion T1-PRT, indicating a parity change of T1. The other transformational motion of T1 involves a "hop" of the 5-atom intervened row onto neighboring edges of the core structure without changing its helicity, corresponding to Figure 2b,c; this motion is named T1-HOP. In T2, two distant Al vacancies in a lateral (111) facet collectively move to its mirror image in the bottom facet with the proper positional change of the 4-atom row, as shown in Figure 2d,e. Because two mirror images form a parity with a mirror plane containing the 3-atom row and perpendicular to the 4-atom row, we named the transformation T2-PRT. The last transformation, named T2-SWP, is a swap of the 3- and 4-atom rows while two vacancies in a bottom facet move to a neighboring facet next to the new 3-atom row, as shown in Figure 2e,f.

Among the seven colored time intervals in Figure 2, we have identified 24 transformational motions of T1 and T2 clusters. Except for a short time interval of T1 at around $t = 700$ ps, the tetrahedral cluster undergoes two to seven successive nanotransformations before surface melting commences. Interestingly, all 24 nanotransformations observed arise through one of the four transformational motions: T1-PRT, T1-HOP, T2-PRT, and T2-SWP. This indicates that the identified surface transformations are elemental motions of the Al_{55} at finite temperature. The time interval between transformations varies from 1.9 to 38.9 ps, with an average value of 17.6 ps. The successive nanotransformations can be effectively represented as a sequence of transitions within two separate configuration spaces of T1 and T2 (Figure 3a−f and legend). Because the tetrahedral cluster has six possible intervened-row positions for a given parity, each space consists of 12 different surface configurations, that is, nodes. Then the observed transitions (e.g., Figure 3e) are pseudorandom trajectories in the *configuration* spaces, similar to the Brownian walk or "jump" in a *real* space.[19]

From the observed trajectories and 6-fold rotational symmetry of the configuration space, we have deduced that the dynamic motion of Al_{55} is the Brownian mo-

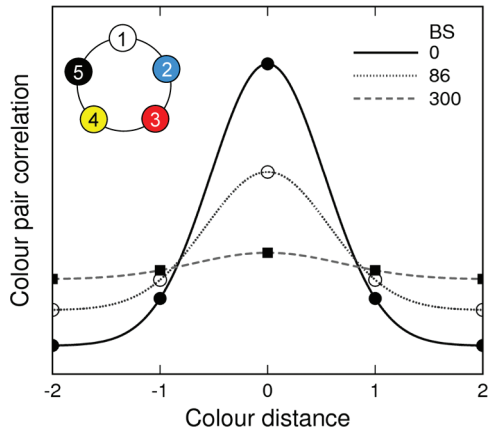

Figure 4. Color diffusion and half-solidity. By assigning color distance between surface atoms, we calculated color pair correlations (CPCs) of the surface of Al_{55} in different Brownian steps (BS = 0, 86, 300). Instead of interatomic distance based on the atomic positions, the color distance was assigned based on the colors of the neighboring atoms in Figure 3H; from the five color codes in the inset ((1) white, (2) blue, (3) red, (4) yellow, (5) black), the color distance, varying from −2 to 2, was determined along the circle in either clockwise (positive) or counterclockwise (negative) way. The CPC distributions for the Brownian steps of 86 and 300 were obtained from ensemble averages of 10 000 Monte Carlo simulations. For eye guide, lines are also plotted.

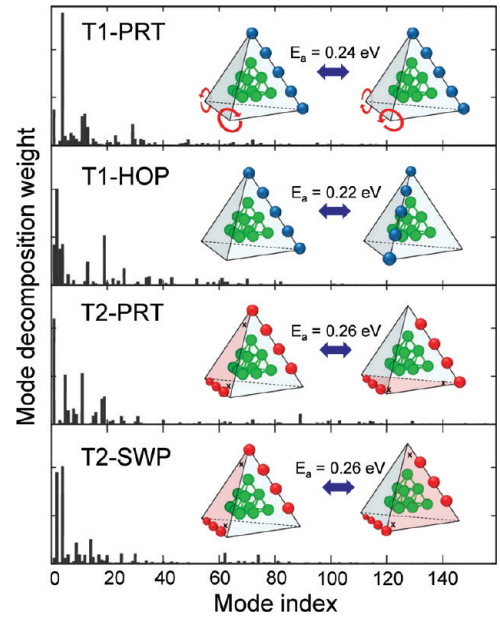

Figure 5. Elemental surface transformations. We calculated inner products between coordinate vectors (from the initial tetrahedral cluster to the saddle-point of each NEB path) and vibrational normal-mode eigenvectors in the 3N-6 dimensional coordinate space for $N = 55$. The normal-mode decomposition weight, defined as a square of the inner products, is plotted for the four elemental motions, T1-PRT, T1-HOP, T2-PRT, and T2-SWP. Insets show the schematic model of the elemental transformations with a tetrahedral pyramid Al_{10} core (green) and intervened rows (blue or red balls). Arrows in the T1-PRT denote the helicity of T1. The pink faces in the T2-PRT and T2-SWP indicate the (111) facet with two vacancies. The calculated activation energy barriers (E_a) are shown.

tion confined within 12-node networks of transformational pathways (Figure 3g). Each link represents a fast pathway for the possible transition. All of the nodes of the T1 network are connected to each other directly or indirectly through another node. On the other hand, the T2 network consists of three disconnected subnetworks, each containing four nodes, which is due to the lack of a hopping motion of the intervened rows (T2-HOP) that is found in the T1-HOP. Because of the small size of the networks, the entropy increase in the nanotransformation is much smaller than that of surface melting. That is why the Brownian motion has a lifetime of about 80 ps at a temperature as high as 550 K. As temperature decreases, *e.g.*, to 400 K, however, the surface melting is less likely, and the intrinsic nanotransformation of Al_{55} prevails in time (see Figure S5 in the Supporting Information).

Each elemental transformation or a Brownian step in the network causes intermixing between constituent atoms of the surface nanodomains. To illustrate the process, we first colored each nanodomain of T1 as shown in the top portion of Figure 3h. After six random steps in the T1 network generated by the Monte Carlo method, the initial structure is transformed to a new T1 structure with the same intervened-row position and the opposite helicity, but with mixed-color domains. After an additional 80 random steps, the initial order of atomic colors largely disappears (Figure 3h, bottom). To quantify the degree of intermixing process, we used color pair correlation (CPC) of surface atoms by defining a color distance between a neighboring pair; the color distance is assigned to zero for two atoms in the same color, while nonzero values are given for other cases depending on their colors (Figure 4 and legend). As a number of Brownian steps increases, an initially sharp peak at zero, arising from the initial order of colors, gets gradually broadened. This strongly indicates that the surface of the Al_{55} cluster is truly a *lattice-liquid* system at the atomic level; the surface atoms on a lattice composed of surface nanodomains evolve or "flow" through the time steps, leading to the diffusion of the CPC distribution (see Figure S6 in the Supporting Information). Therefore, the Al_{55} cluster at finite temperature is in an unprecedented dynamic state (termed as *half-solidity*) that is in a delicate balance between order and disorder.

Finally, we have analyzed the four elemental motions, T1-PRT, T1-HOP, T2-PRT, and T2-SWP, to understand microscopic and dynamical mechanisms of the half-solidity.

Microscopic Mechanism. A symmetry mismatch between the core and surface structure of tetrahedral Al_{55} clusters makes the surface transformations possible with low transition energy barriers. Compared to the tetrahedral pyramid Al_{10} core with a high symmetry (T_d), the surface of the tetrahedral cluster has a reduced or broken symmetry in the presence of intervened rows, helicity of surface, and intrinsic vacancies. This symmetry

mismatch affects stacking of the (111) Al_{10} facet on the fcc-like Al_{10} core, weakening bonds between the surface and the core atoms. With the nudged elastic band (NEB) method,[20] the activation energy barriers (E_a) of T1-PRT, T1-HOP, T2-PRT, and T2-SWP are calculated to be 0.24, 0.22, 0.26, and 0.26 eV, respectively. These energy barriers are sufficiently small that the elemental transformations can be thermally activated effectively at temperatures below the main melting temperature. We also considered T2-HOP and surface transformation from T1 to T2 to understand why such motions are not observed directly in our 1.5-ns MD simulation. The calculated activation energy barriers are 0.86 and 0.60 eV for the T2-HOP and T1-T2 conversion, respectively (see Figure S7 in the Supporting Information). Therefore, these motions are secondary rare events.

Dynamical Mechanism. Why and how do the elemental motions, which need collective rearrangements of surface atoms, emerge during random vibrations of individual atoms? To answer this question, we decomposed the NEB paths onto vibrational normal-mode eigenvectors of Al_{55} in Figure 5. The high weight distribution to a few small mode indexes indicates that each elemental transformation can be described in terms of large-amplitude thermal excitations of the soft normal modes. The soft normal modes correspond to in-phase collective motions of constituents. Although the average potential energy per each vibrational mode is only 24 meV at $T = 550$ K by the equipartition theorem, a small number of vibrational modes among 159 modes happen to have much larger energy by fluctuations. This is thus a characteristic of nanosystems.

Then, the transformation rate γ is estimated by the relation $\gamma \approx \omega_{soft} \exp(-E_a/k_BT)$ with activation energy barrier $E_a \approx 0.25$ eV and quasi-normal-mode frequency $\omega_{soft} \approx 10^{13}$ Hz from the calculated phonon spectrum. The rate at $T = 550$ K is 1/19.5 ps, in good agreement with the average time interval of 17.6 ps observed. At $T = 400$ K, the calculated rate γ decreases to 1/141 ps, consistent with a direct MD simulation result of 1/123 ps (see Figure S5 in the Supporting Information).

Flexible solidity as represented by collective transformations can be general in nanosystems. We have noticed a striking mapping between dynamics of two ostensibly different nanosystems—Al_{55} and ubiquitin (a small regulatory protein[21] comprising 76 amino acids): (i) A recent analysis by Lange *et al.*[22] revealed that ubiquitin in solution undergoes spontaneous structural conversion among 46 slightly different conformations just below its melting temperature ($T \approx 0.9T_m$), as does the Al_{55} between 12 different configurations. On time scales relevant to the protein dynamics, each amino acid serves as more or less a constituent particle.[23] (ii) Similar to the Al_{10} core, the protein has rigid hotspot residues as its protein core, with the secondary structures being nanodomains. (iii) The conformational change is mainly attributed to a single collective mode of residues, corresponding to our collective or soft phonon modes of elemental motions. The dynamic conformational change under the near-T_m fluctuations enables stochastic, selective molecular recognition with flexible functionality[22,24] rather than deterministic, induced-fit motions.

CONCLUSION

In conclusion, using first-principles molecular dynamics simulations we have found exotic, but intrinsic, nanotransformations of a tetrahedral Al_{55} cluster below its melting temperature. The Al_{55} cluster in a thermal environment constantly undergoes structural changes—such as a change of helicity or a movement of intervened rows. This intrinsic thermal motion is governed by the Brownian dynamics confined within a well-defined network of transformational pathways, and characterized as a half-solidity state with structural order but color shuffling. The half-solidity, observed as a new form of flexible solid state, will provide valuable insight into understanding the stability and functionality of finite-size grained systems in nanoscience and molecular biology.

METHODS

Total energies and Hellmann−Feynman forces were calculated within the generalized gradient approximation (GGA-PBE[25]) to the density functional theory, using projector-augmented wave potentials, as implemented in the VASP package.[26,27] First-principles molecular dynamics simulations were performed in the canonical ensemble at constant temperatures, with the Nosé thermostat[28] and the time step of 3 fs. Heat capacity was calculated using the multiple-histogram method[2,11] (see the Supporting Information). Activation energy barriers of the elemental transformations (T1-PRT, T1-HOP, T2-PRT, and T2-SWP) were determined with the nudged elastic band method.[20] The detailed atomic movements along the NEB paths as movies and the atomic coordinates of T1 and T2 are provided in the Supporting Information.

Acknowledgment. We thank S.-H. Wei and D. Blake for discussions and for reading the manuscript. This work was funded by the DOE EERE CSP and NREL LDRD programs under Contract No. DE-AC36-08GO28308. Y.-H. Kim was also supported by WCU (World Class University) program through the National Research Foundation of Korea funded by the Ministry of Education, Science and Technology (R31-2008-000-10071-0).

Supporting Information Available: Simulation details, supporting figures, movies, and the coordinates of the ground-state structures. This material is available free of charge *via* the Internet at http://pubs.acs.org.

REFERENCES AND NOTES

1. Filinov, A. V.; Bonitz, M.; Lozovik, Y. E. Wigner Crystallization in Mesoscopic 2D Electron Systems. *Phys. Rev. Lett.* **2001**, *86*, 3851–3854.

2. Labastie, P.; Whetten, R. L. Statistical Thermodynamics of the Cluster Solid−Liquid Transition. *Phys. Rev. Lett.* **1990**, *65*, 1567–1570.
3. Matsuoka, H.; Hirokawa, T.; Matsui, M.; Doyama, M. Solid−Liquid Transitions in Argon Clusters. *Phys. Rev. Lett.* **1992**, *69*, 297–300.
4. Cheng, H.-P.; Berry, R. S. Surface Melting of Clusters and Implications for Bulk Matter. *Phys. Rev. A* **1992**, *45*, 7969–7980.
5. Kunz, R. E.; Berry, R. S. Coexistence of Multiple Phases in Finite Systems. *Phys. Rev. Lett.* **1993**, *71*, 3987–3990.
6. Schmidt, M.; Kusche, R.; v. Issendorff, B.; Haberland, H. Irregular Variations in the Melting Point of Size-Selected Atomic Clusters. *Nature* **1998**, *393*, 238–240.
7. Breaux, G. A.; Neal, C. M.; Cao, B.; Jarrold, M. F. Melting, Premelting, and Structural Transitions in Size-Selected Aluminum Clusters with Around 55 Atoms. *Phys. Rev. Lett.* **2005**, *94*, 173401.
8. Proykova, A.; Berry, R. S. Insights into Phase Transitions from Phase Changes of Clusters. *J. Phys. B* **2006**, *39*, R167–R202.
9. Noya, E. G.; Doye, J. P. K.; Calvo, F. Theoretical Study of the Melting of Aluminum Clusters. *Phys. Rev. B* **2006**, *73*, 125407.
10. Zhang, W.; Zhang, F.; Zhu, Z. Molecular Dynamics Study on the Melting Phase Transition of Aluminum Clusters with Around 55 Atoms. *Phys. Rev. B* **2006**, *74*, 033412.
11. Chandrachud, P.; Joshi, K.; Kanhere, D. G. Thermodynamics of Carbon-Doped Al and Ga Clusters: *Ab Initio* Molecular Dynamics Simulations. *Phys. Rev. B* **2007**, *76*, 235423.
12. Starace, A. K.; Neal, C. M.; Cao, B.; Jarrold, M. F.; Aguado, A.; López, J. M. Correlation between the Latent Heats and Cohesive Energies of Metal Clusters. *J. Chem. Phys.* **2008**, *129*, 144702.
13. Vaitheeswaran, S.; Yin, H.; Rasaiah, J. C.; Hummer, G. Water Clusters in Nonpolar Cavities. *Proc. Natl. Acad. Sci. U.S.A.* **2004**, *101*, 17002–17005.
14. Prabhu, N. V.; Sharp, K. A. Heat Capacity in Proteins. *Annu. Rev. Phys. Chem.* **2005**, *56*, 521–548.
15. Chung, H. S.; Khalil, M.; Smith, A. W.; Ganim, Z.; Tokmakoff, A. Conformational Changes during the Nanosecond-to-Millisecond Unfolding of Ubiquitin. *Proc. Natl. Acad. Sci. U.S.A.* **2005**, *102*, 612–617.
16. Lei, H.; Wu, C.; Liu, H.; Duan, Y. Folding Free-Energy Landscape of Villin Headpiece Subdomain from Molecular Dynamics Simulations. *Proc. Natl. Acad. Sci. U.S.A.* **2007**, *104*, 4925–4930.
17. Xu, W.; Kong, J. S.; Yeh, Y.-T. E.; Chen, P. Single-Molecule Nanocatalysis Reveals Heterogeneous Reaction Pathways and Catalytic Dynamics. *Nat. Mater.* **2008**, *7*, 992–996.
18. Li, X.; Wu, H.; Wang, X.-B.; Wang, L.-S. s-p Hybridization and Electron Shell Structures in Aluminum Clusters: A Photoelectron Spectroscopy Study. *Phys. Rev. Lett.* **1998**, *81*, 1909–1912.
19. Nykypanchuk, D.; Strey, H. H.; Hoagland, D. A. Brownian Motion of DNA Confined within a Two-Dimensional Array. *Science* **2002**, *297*, 987–990.
20. Mills, G.; Jónsson, H.; Schenter, G. K. Reversible Work Transition State Theory: Application to Dissociative Adsorption of Hydrogen. *Surf. Sci.* **1995**, *324*, 305–337.
21. Nath, D.; Shadan, S. The Ubiquitin System. *Nature* **2009**, *458*, 421.
22. Lange, O. F.; Lakomek, N.-A.; Farès, C.; Schröder, G. F.; Walter, K. F. A.; Becker, S.; Meiler, J.; Grubmüller, H.; Griesinger, C.; de Groot, B. L. Recognition Dynamics up to Microseconds Revealed from an RDC-Derived Ubiquitin Ensemble in Solution. *Science* **2008**, *320*, 1471–1475.
23. Tozzini, V. Coarse-Grained Models for Proteins. *Curr. Opin. Struct. Biol.* **2005**, *15*, 144–150.
24. Eisenmesser, E. Z.; Millet, O.; Labeikovsky, W.; Korzhnev, D. M.; Wolf-Watz, M.; Bosco, D. A.; Skalicky, J. J.; Kay, L. E.; Kern, D. Intrinsic Dynamics of an Enzyme Underlies Catalysis. *Nature* **2005**, *438*, 117–121.
25. Perdew, J. P.; Burke, K.; Ernzerhof, M. Generalized Gradient Approximation Made Simple. *Phys. Rev. Lett.* **1996**, *77*, 3865–3868.
26. Kresse, G.; Furthmüller, J. Efficient Iterative Schemes for *ab Initio* Total-Energy Calculations Using a Plane-Wave Basis Set. *Phys. Rev. B* **1996**, *54*, 11169–11186.
27. Kresse, G.; Joubert, D. From Ultrasoft Pseudopotentials to the Projector Augmented-Wave Method. *Phys. Rev. B* **1999**, *59*, 1758–1775.
28. Nosé, S. A. A Unified Formulation of the Constant Temperature Molecular-Dynamics Methods. *J. Chem. Phys.* **1984**, *81*, 511–519.